International Journal of Power Electronics and Drive System (IJPEDS)
Vol. 17, No. 3, September 2026, pp. 1926~1940
ISSN: 2088-8694, DOI: 10.11591/ijpeds.v17.i3.pp1926-1940

Modeling and four-loop master–slave control of a six-phase interleaved buck converter for ultrafast EV charging

Alya H. Al-Rifaie[1,2], Mohammed Obaid Mustafa[1]
[1]Department of Electrical Engineering, College of Engineering, University of Mosul, Mosul, Iraq
[2]Department of Electrical Engineering Techniques, Technical Engineering College/Mosul,
Northern Technical University, Mosul, Iraq

Article Info

Article history:

Received Dec 12, 2025
Revised Jul 13, 2026
Accepted Aug 14, 2026

Keywords:

Four-loop control
IBC
Master-slave strategy
SIDO
Ultrafast charging

ABSTRACT

In this paper, modeling and control of a six-phase interleaved buck converter (IBC) are presented for fast charging of ultra-fast electric vehicle (EV) batteries. The primary difficulty faced is the need to operate at high power charging rates with stable and efficient performance, while minimizing output ripple and current sharing errors. To solve these problems, the cascaded multi-loop control method is proposed using a proportional-integral (PI) controller. By implementing a reduced number of control loops (four coordinated loops) from conventional configurations, the control structure is simplified, while stable operation and effective current sharing are maintained. The proposed system is implemented in a constant current/constant voltage (CC-CV) charging method, which guarantees safe and efficient battery charging. The proposed system is validated by using MATLAB/Simulink simulation under steady-state and transient conditions. The results show that with a very small amount of ripple, a battery voltage of about 820 V and a charging current of 330 A are obtained. The dynamic response has a settling time of about 100 ms and an overshoot less than 5%, which is suitable for disturbances. Furthermore, in the SIMO configuration, it is noted that a disturbance or fault on the output of one of the cascaded control loops has minimal effect on the output of the other control loop, which illustrates good decoupling between cascaded control loops. This is a sign of better robustness and reliability for multi-output EV charging applications. Moreover, the stability margins of the proposed control method are verified by frequency-domain analysis.

Corresponding Author:

Alya H. Al-Rifaie
Department of Electrical Engineering, College of Engineering, University of Mosul
Al-Minsaa St, Mosul City, Nineveh Governorate, Iraq
Email: alya.23enp10@student.uomosul.edu.iq, alya.hamid@ntu.edu.iq

1. INTRODUCTION

The increasing fleet of EVs demands a simultaneous setup of battery charging stations. Consequently, the battery charging infrastructure has a significant role to play in the achievement of the electrification of transportation fleets. However, with current technology, EV battery charging takes hours, and slow charging technologies do not fulfil all drivers' requirements, particularly for medium and long-distance trips. Accordingly, the need for reduced charging times has fueled research into fast and ultra-fast charging technology to reduce the charging time needed for more extensive use of EVs. As part of the effort to cut charging times for EV batteries, more and more people are talking about increasing EV charger nominal power. The need for chargers to provide an ultrafast charging infrastructure is leading to a trend of higher nominal power for EV chargers. In this instance, a high-power output and a wide range of output voltage (DC-DC switching) converter circuit needs to have high efficiency. Another method to boost the output power is to connect DC-DC switching converters in parallel. If used in parallel to perform the replication of many DC-DC switching converters, the power that can be handled is higher compared to a single DC-DC converter topology, and therefore the modular structure is more convenient for the ultra-fast charging of EV batteries. The additional advantages are increased power density, better thermal management, and increased efficiency [1]. Also, by applying a proper control strategy robust to uncertainties, with a suitable high priority assigned to robustness and reliability, the output voltages can be achieved over a wide range.

They are valuable benefits for the future development of the ultrafast EV charging infrastructure worldwide, facilitating EV users in their efforts to reduce carbon emissions. Also, a non-isolated converter can be used as the DC bus-to-EV battery interface for charging stations with a single charging point and galvanic isolation in the electrical layout. The converter's primary function is to charge the EV battery; thus, it should be unidirectional [2]. The use of interleaved operation has been well studied in the output stage of off-board EV battery chargers. A recent study [3] presented a simulation of a 36-phase 350 kW IBC rated for an 800 V battery charged from a 1500 V DC bus with a charging time of less than 10 minutes for an ultrafast EV battery charging application. The results showed that in practical applications, high power capability, low output voltage and current ripples, and better overall performance can be achieved. Likewise, the modeling and characterization of N-phase IBC was studied in [4], where an N-1 stability analysis of three different configurations: single-phase, two-phase, and three-phase was performed. The results showed that the three-phase IBC is much more stable than the single-phase converter, especially for the case of parasitic elements. The 3-phase interleaved topology also provides reduced conduction losses. The analysis of the previous work, however, dealt only with resistive loads and rheostatic experiments and did not cover the practical battery charging conditions. Other works [5]–[12] have investigated the implementation of two-phase IBC synchronous charging in Li-ion batteries using a closed-loop controller with microcontroller implementation. Based on these studies, interleaved DC-DC converter operation results in better charging efficiency and a smooth output voltage.

This paper investigates the modular configuration of DC–DC power units based on IBC for ultrafast electric vehicle (EV) battery charging applications. The primary objective is to develop a simplified model of a six-phase IBC under ideal conditions, serving as the foundation for a systematic control design tailored to a battery-charging system using this topology. The secondary objective is to design a control scheme capable of regulating the inductor current across all six phases while accounting for the interleaving effect and simultaneously managing the charging process according to a predefined protocol. The suggested control method is organized in a four-loop cascaded architecture and uses pulse-width modulation (PWM). In order to correct current imbalance between various phases, the innermost control loop uses the democratic current-sharing technique and controls the inductor currents. This is accomplished by putting in place separate proportional-integral (PI) controllers for every phase, each of which shares a reference produced by the voltage control loop. The (CC–CV) charging protocol is implemented by the three outer control loops: the outermost loop controls the battery current through a saturation block that restricts its control action, while the inner loop controls the output voltage. The transition from the CC mode to the CV mode occurs smoothly once the output voltage reaches the target level.

A wide range of studies have investigated the control of IBC. The studies [13]–[19] introduce methodologies for designing passive components in such converters; however, the associated control design strategies are not elaborated. An alternative modeling and implementation approach for IBC is presented in [20], where a direct relationship between each inductor leg current and its corresponding switch duty cycle is established. In this framework, the total output reference current is divided among the converter legs, and each phase independently regulates its inductor current. Meanwhile, [21] provides an averaged analysis of inductor current sharing, and [22] examines the bandwidth limitations of IBC control loops. Nevertheless, the digital implementation aspects of IBC control remain insufficiently addressed in existing literature. In this context, the present work proposes detailed control designs for a 60 kW IBC intended for fast battery charging stations. The total output current control and inductor current sharing control are treated as distinct but coordinated problems. The corresponding controllers are developed and analyzed first in the continuous-time (ω) domain and subsequently transformed into the discrete-time (z) domain. Although a lot of research has been conducted on IBC for EV charging applications, there are still some issues that need to be addressed, such as current sharing, voltage regulation, and coordinated control in multi-output charging. The majority of the available studies are based on single-output systems or simplified control strategies and do not consider integrated multi-loop control structures to be able to achieve a dual-output operation. To overcome the drawbacks of the above, this paper suggests a four-loop cascaded master–slave control method for a 6-phase IBC. The proposed approach is not restricted to reducing the current ripple as it is done using interleaving, but it can also simplify the cascaded control architecture, decrease the number of coordinated control loops from six to four, reduce the complexity of implementation, and achieve accurate current sharing as well as stable CC–CV regulation and fast dynamic performance. Also, the proposed controller is capable of both single-input single-output (SISO) and single-input dual-output (SIDO) operation, maintaining a dynamic decoupling between the two outputs, which results in a negligible impact of disturbance on the output of the other channel. The validity of the proposed architecture is confirmed by detailed MATLAB/Simulink simulations, showing the feasibility of the architecture for scalable and reliable ultra-fast EV charging applications. Future work will comprise experimental validation of the proposed methods with hardware-in-the-loop (HIL) platforms. The remainder of this paper is organized as follows: i) A thorough system description and mathematical modeling are presented in section 2, which is followed by a dynamic analysis based on the six-phase IBC's small-signal model; ii) In section 3, the four-loop control strategy is examined. The controller employs three outer loops for the CC-CV charging protocol, and an inner loop for current sharing among the 6 phases in the inductor. MATLAB simulation is again used to ensure proper functioning of the control system in the same section; iii) Input and load disturbances and parameter uncertainties with the converter are considered in a robustness test of the controller in section 4; and iv) Lastly, conclusions are presented in section 5.

2. EXPLANATION OF CIRCUITS AND MATHEMATICAL MODELING

2.1. Research methodology

In this work, a simulation-based method is used to study the performance of the 6-phase IBC for ultrafast EV charging applications. This is suitable because of the high-power level, the complexity of the system, and the fact that the simulation serves as a flexible and safe environment for system analysis and control design. The system is modeled and implemented in MATLAB/Simulink, and the converter topology, battery model, and control loops are designed according to the normal ultrafast charging requirements. There are a number of steps involved in the study. The derivation of the mathematical model of the converter is done first. Second, the control strategy is developed using a four-loop cascaded control scheme. Thirdly, steady-state and disturbance simulations of the system are performed to assess the performance of the system. To achieve accurate current sharing and stable voltage regulation, the proposed control strategy uses master–slave control and PI controllers. Key performance indicators like voltage regulation, current sharing accuracy, settling time, and disturbance rejection are evaluated for system performance validation.

2.2. Circuit explanation

The suggested circuit, illustrated in Figure 1, can be implemented in either a single-output or a dual-output configuration. In the single-output configuration, all N IBC phases operate in parallel to supply the same battery or load. In the dual-output configuration, the N phases are divided into two groups, each powering an independent battery pack or load. Both groups share the same DC input voltage vin but are controlled by independent regulation loops to meet the changing requirements of each load. Within each group, a phase shift of $\frac{2\pi}{N}$ between the PWM gate signals ensures symmetric interleaving and minimizes current ripple.

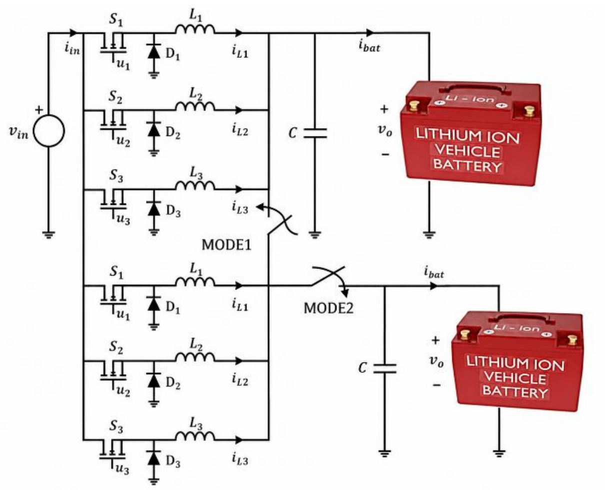

Figure 1. Six-phase IBC SISO/DO

2.3. Mathematical model

The voltage and current balancing equations for the ON and OFF switching states are derived to provide the mathematical model of the converter. The variables (u_1, u_2,..., u_N), which take binary values 1 for the ON state and 0 for the OFF state, are used to represent both operating states. This results in the system of equations shown in (1).

$$\frac{di_{L1}}{dt} = \frac{v_{in}}{L_1} u_1 - \frac{v}{L_1}$$

$$\frac{di_{L2}}{dt} = \frac{v_{in}}{L_2} u_2 - \frac{v}{L_2}$$

$$\frac{di_{LN}}{dt} = \frac{v_{in}}{L_N} u_N - \frac{v}{L_N}$$

$$\frac{dv}{dt} = \frac{i_{L1}+i_{L2}+\cdots+i_{LN}}{C} - \frac{v}{R_b C} + \frac{v_b}{R_b C} \tag{1}$$

Where the control signals are S_1, S_2, S_N, and u_1, u_2, u_N, and so on. The primary goals of this work are to precisely synthesize each controller of the four-loop control system and construct a high-power battery charger based on a 6-phase IBC capable of producing 270 kW to charge an 820 V battery. In addition to the single-output operation, the proposed converter can also be configured for dual-output operation by dividing the six phases into two independent groups. In this case, the control architecture employs four loops in total: one current-control loop, two voltage-control loops (one for each output), and one current-sharing loop to ensure uniform distribution among the phases. Thus, the dual-output structure is realized simply by adding a second voltage-control loop while reusing the same current-control and current-sharing loops. The first step in the design process is to study the dynamics of the converter illustrated in Figure 1 and to derive the corresponding small-signal model. For this purpose, the following assumptions are made: all phase inductances are equal, i.e., $L_1 = L_2 = \cdots = L_N = L$; passive components and semiconductor devices are assumed ideal; and the open-circuit voltage V_{bat} of the battery model is assumed constant for controller design, while allowed to vary with the state of charge (SoC) in numerical simulations.

$$\frac{di_L}{dt} = \frac{v_{in}}{L_1} u - \frac{v}{L} \tag{2}$$

$$\frac{dv}{dt} = \frac{Ni_L}{C} - \frac{v}{R_b C} + \frac{v_b}{R_b C} \tag{3}$$

The averaged model is derived by assuming identical inductance values and substituting the control variables u_1, u_2, …, u_N in (1) with their average value, which corresponds to the duty cycle d.

2.4. Small signal model

By inserting small perturbations into the variables in (2) and (3), linearizing and applying the Laplace transform, the small signal model of the system is obtained as expressed in (4) and (5).

$$\widetilde{V}(s) = \tilde{d}(s)\frac{v_{in}\frac{N}{LC}}{d_n} + \widetilde{V_{in}}(s)\frac{D\frac{N}{LC}}{d_n} + \widetilde{V_b}(s)\frac{\frac{1}{R_b C}S}{d_n} \tag{4}$$

$$\tilde{I}(s) = \tilde{d}(s)\frac{\frac{v_{in}}{L}\left(s+\frac{1}{R_b C}\right)}{d_n} + \widetilde{V_{in}}(s)\frac{\frac{D}{L}\left(s+\frac{1}{R_b C}\right)}{d_n} - \widetilde{V_b}(s)\frac{\frac{1}{LR_b C}}{d_n} \tag{5}$$

Where $d_n = S^2 + \frac{1}{R_b C}S + \frac{N}{LC}$.

Specifically, the control-to-output voltage transfer function $G_{dv(s)} = \frac{\widetilde{V}(s)}{\tilde{d}(s)}$ and the control-to-inductor current transfer function $G_{di(s)} = \frac{\tilde{I}(s)}{\tilde{d}(s)}$ can be expressed as (6) and (7).

$$G_{dv(s)} = \frac{\widetilde{V}(s)}{\tilde{d}(s)} = \frac{1}{LC}\frac{6v_{in}}{S^2+\frac{1}{R_b C}S+\frac{6}{LC}} \tag{6}$$

$$G_{di(s)} = \frac{\tilde{I}(s)}{\tilde{d}(s)} = \frac{v_{in}}{L}\frac{\left(s+\frac{1}{R_b C}\right)}{S^2+\frac{1}{R_b C}S+\frac{6}{LC}} \tag{7}$$

The (6) and (7) are the transfer functions from the control to the output voltage and the transfer function from the control to the current through the inductor, respectively. The next four-loop cascaded PI controller design in Section 3 is based on these transfer functions. In accordance with the cascade control principle, the inner current loop is designed to have a fast dynamic response, while the outer voltage and battery-current loops are designed to control the CC–CV charging and to ensure the stability of the system operation. Each output step in the dual-output arrangement has a mathematical model that is comparable to the single-output scenario. The N interleaved phases are separated into two groups: N1 phases provide output 1, and N2=N−N1 phases provide output 2. Each group functions as a separate IBC, controlling its own output voltage and current in accordance with the specific load or battery requirements while sharing the same input voltage Vin. To guarantee symmetric interleaving, lower current ripple, and boost overall efficiency, a fixed phase-shift of $\frac{2\pi}{N_1}$ for output 1 and $\frac{2\pi}{N_2}$ for output 2 is applied between the gate signals within each group. As a result, each group's state-space equations have the same form as the single-output model, with output 1's corresponding parameters and variables (Lk, C1, Vo1, Iload1) and (Lm, C2, Vo2, Iload2) for output 2, the state-space equations for each group thus have the same form as the single-output model. This makes it possible to generate the dual-output model by simply repeating the single-output equations for each group using the proper notation.

2.5. Component design and practical considerations

However, in practical applications, the IBC is affected by the non-ideal properties of the components, such as switching losses and parasitic resistances, and thermal effects. These factors add to the losses and impact reliability and efficiency. Ripple constraints and system specifications are used to design the passive components. The inductance value is determined as in (8) [22], [23].

$$L = \frac{(V_{in} - V_{out}).D}{6\,\Delta I_L\,.f_s} \tag{8}$$

This is because ΔI_L is the maximum current ripple allowed in the inductor, which is usually set at 20% of the rated current. Likewise, the output capacitance is determined as in (9).

$$C = \frac{\Delta I_L}{48\ f_s\ \Delta V_{out}} \tag{9}$$

The factor (6) represents the number of interleaved phases, and ΔV_{out} is the acceptable voltage ripple on the output. Selected values of L and C provide low ripple, stable operation, and reliable performance under high power conditions. Furthermore, there are thermal limits and thermal constraints to ensure safe and efficient operation.

In the present study, an ideal converter model is considered for the development of the controller. There are some practical constraints that are not included, such as parasitic resistances, semiconductor switching losses, thermal considerations, magnetic saturation, and device rating, which will be discussed in the upcoming experimental studies.

3. CONTROLLER DESGIN

The comprehensive control structure of the suggested battery charger is illustrated in Figure 2. The system differentiates a multiple-loop controller. The inner loop controls the inductor currents and provides for correct sharing of the currents between the interleaved phases. The outer loops control the battery current and output voltage, using the (CC–CV) charging protocol. The proposed control strategy can be used for the SISO case and the SIDO case, thus allowing flexible operation and independent control of the multiple outputs.

The transfer functions were used to specify the parameters for the PI controller, alongside the converter design parameters: input voltage V_{in}, inductance L, output capacitance C, battery resistance $R_{b,}$ and the switching frequency f_s. These parameters are the converter dynamics to be used to calculate the bandwidth, damping factor, and natural frequency of the controller for the desired overshoot and settling time. The inner current loop was designed first, then the outer voltage and battery current loop was designed with successively lower bandwidths, following the cascade control principle. This resulted in the PI gains, finally verified by MATLAB/Simulink simulation, which are summarized in Table 2.

3.1. Inner loop controller design

The 6-phase IBC is designed with the vision of a democratic current sharing control to distribute the current equally among the phases. All 6-phases are equal for the same reason as the inductances, and because we are not considering any parasitic resistances. Hence, the inductor current of each phase is controlled by a similar PI controller $GP3(s)$. So, the duty cycle for each converter is similar, but the phase shift for SISO and SIDO is 60° and 120°, respectively. The block diagram of the inner loop, with the consideration of the dynamic current model provided in (5), is given in Figure 3.

Maximum overshoot, steady-state error, and settling time are specified while designing the control parameters KP3 and τi3. These parameters can be obtained analytically by first designing the system to have the optimal performance and reliability characteristics within the expected range of operating conditions by determining the natural frequency and damping coefficient.

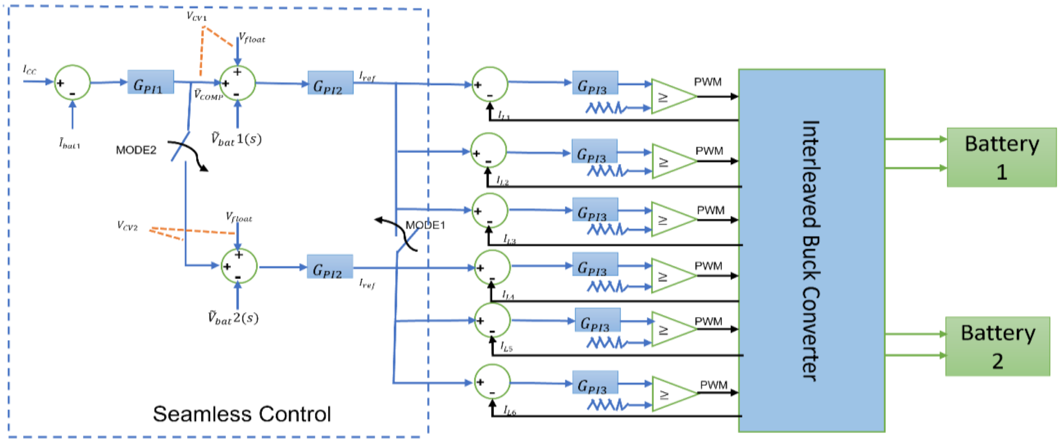

Figure 2. Complete scheme of the proposed cascade (multistage) controller structure

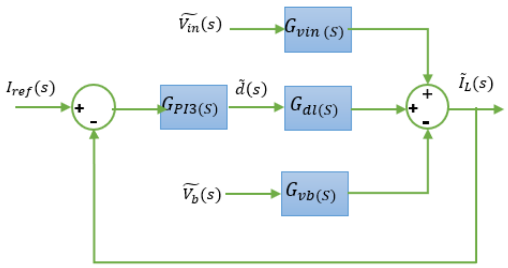

Figure 3. Block diagram of the multiphase IBC's current dynamic model

3.2. Design of the controller for the outer voltage battery loop

Figure 4 illustrates the cascade control structure for both single-output and dual-output configurations. In Figure 4(a), corresponding to the SISO case, the block diagram shows the battery voltage control loop and its relationship with the inductor current loop, where the reference signal $\tilde{V}_{CV}(s)$ is obtained as the summation of $\tilde{V}_{com(s)}$ and V_{float}. Following cascade control design principles, the inner current loop is designed to be at least an order of magnitude faster than the outer voltage loop. Based on this, the voltage controller $G_{PI2}(s)$ is synthesized by specifying performance indices such as steady-state error, settling time, and overshoot, while the transfer function $Gv(s)$ is derived from the closed-loop current dynamics represented by $Gd(s)$.

In Figure 4(b), the structure is extended to the SIDO case, where the same master–slave current loop governs the total charging current, while two independent voltage control loops regulate the terminal voltages of each battery, $V_{bat1(s)}$ and $V_{bat2(s)}$. Each voltage reference is generated by combining its own $\tilde{V}_{com(s)}$ and floating voltage term, allowing seamless CC–CV transitions for both outputs. This dual configuration provides a unified framework capable of achieving balanced current distribution and independent voltage regulation in multi-battery EV fast-charging scenarios.

$$G_v(s) = G_{dv}(s)\frac{G_{PI3}(s)}{1+G_{PI3}G_{di}(s)} \tag{10}$$

The voltage controller is then designed using the same technique, taking into account the maximum overshoot and settling time specifications.

3.3. Design of the outer battery current loop controller

The battery current is controlled by the external loop. The block diagram of the battery voltage loop in cascade with the battery current control loop for the single-output (SISO) scenario is shown in Figure 5(a). The first step in designing the current controller $G_{P1}(s)$ is to create the closed voltage-loop transfer function $G_{cl-v}(s)$.

$$G_{cl-v}\,(s) = \frac{G_v(s)\times G_{PI2}(s)}{1+G_V(s)\times G_{PI2}(s)} \tag{11}$$

As shown in the block diagram, the relationship between battery voltage and current is expressed as (12):

$$\frac{\tilde{I}_{bat}(s)}{\tilde{V}_{bat}(s)} \tag{12}$$

where Rb represents the battery equivalent resistance. The voltage loop is considered the inner loop and must operate at least an order of magnitude faster than the outer current loop to guarantee stability and proper cascade performance.

In Figure 5(b), the structure is extended to the dual-output (SIDO) configuration. In this case, a master–slave control strategy is applied, where the outer current loop regulates the total charging current with reference to the master battery, while the slave battery is inherently coordinated within the same loop. Two independent voltage loops are then responsible for controlling the terminal voltages of each battery, thus ensuring a seamless CC–CV transition for both outputs. Although the general design method follows standard practices in power electronic applications, the novelty of this work lies in applying the cascaded control framework to the context of ultrafast EV battery charging, where coordinated SISO and SIDO operation enables robust current regulation, accurate voltage control, and smooth CC–CV implementation.

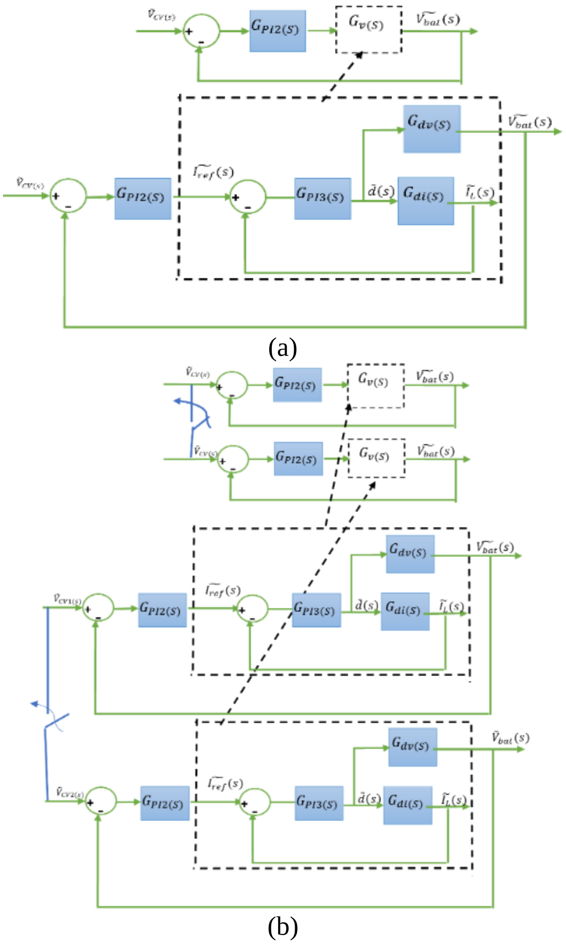

Figure 4. Voltage and inductor current cascade controller block diagram: (a) SISO and (b) SIDO

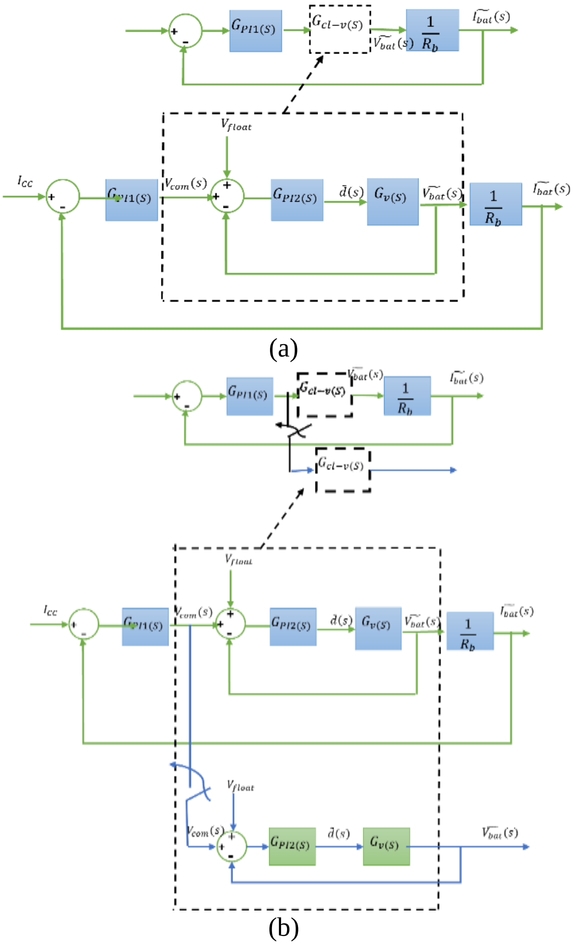

Figure 5. Battery current and voltage cascade controller block diagram: (a) SISO and (b) SIDO

Frequency domain analysis is used to verify the stability of the proposed control system. Figure 6 and Figure 7 show the Bode plots of the current and voltage control loops, respectively. The phase margin of the current loop is around 90°, which indicates a very stable and quick dynamic response. The voltage loop, on the other hand, exhibits a phase margin of approximately 72.8°, resulting in stable voltage regulation and sufficient damping.

Further, the hierarchy of the control loops ensures the correct dynamic decoupling; that is, the bandwidth of the inner current loop is higher than the outer voltage loop, and thus the system is more stable and has a better transient response. In addition, the proposed control strategy can be realized with low complexity of computation and simple PI-based structure on a digital platform such as a DSP or an FPGA.

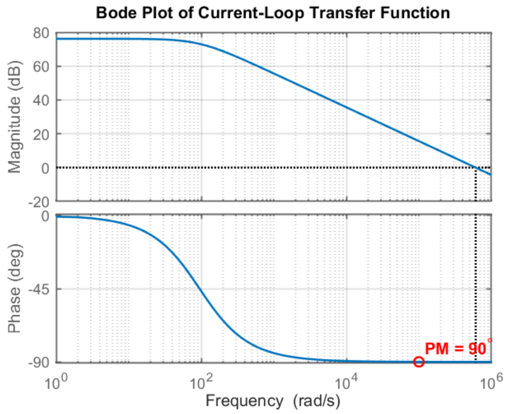

Figure 6. Bode plot of the current-loop transfer function showing phase margin

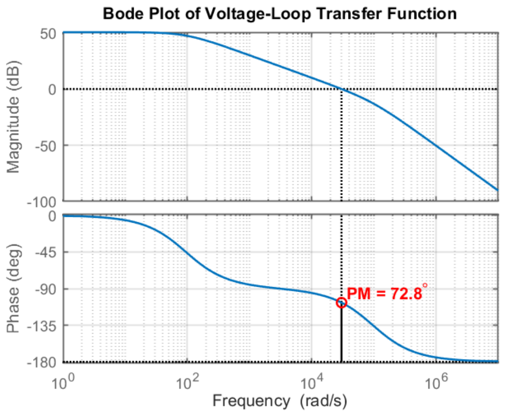

Figure 7. Bode plot of the voltage-loop transfer function showing phase margin

4. RESULTS AND DISCUSSION

4.1. Steady-state response

The system parameters listed in Table 1 and the PI parameters listed in Table 2 have been used in MATLAB to simulate the battery charger designed on the IBC of Figure 2. The parameters for the inner controller PI3 are found by designing the controller to have a maximum overshoot of 2-5% and a settling time of 0.5-1 ms. With reference to the cascade configuration, an overshoot of 3% and 2% and a settling time of 5–20 ms and 20 – 60 ms were selected for the PI2 and PI1 designs, respectively.

Table 1. System parameters

Parameter	Value	Parameter	Value
Input voltage	2000 V	Switching frequency	20 KHz
Battery voltage range	400-820 V	Inductance	3.3 mH
Battery current	330 A	Output capacitance	200 µF
Battery capacity	133 Ah	Battery resistance	0.052 Ω

Table 2. Controller parameters

Controller	Kp	KI
PI_3	0.0207	52.112
PI_2	0.376	142.122
PI_1	0.05	5

Figure 8 shows the steady-state waveforms of the battery current, output voltage, and inductor currents of the interleaved phases. The results demonstrate that the system achieves stable operation with a battery voltage of approximately 820 V and a charging current of 330 A. In addition, both voltage and current exhibit very low peak-to-peak ripple, confirming the effectiveness of the interleaved structure in reducing current stress and improving output quality.

Figure 9 presents the steady-state performance under dual-output operation, where the battery current is equally shared at 165 A while maintaining the output voltage at 820 V. The results confirm proper current sharing and independent voltage regulation, with minimal ripple due to the phase-shifted operation of the interleaved converter.

The achieved steady-state performance is consistent with the stability analysis of current and voltage control loops presented in section 3 where adequate phase margins were obtained for both loops. The outcomes demonstrate the efficacy of the proposed cascaded control strategy in sustaining stable operation, accurate current sharing, and minimal ripple, all of which are crucial for achieving the high performance of an EV charging system. Moreover, the dual-output mode shows the flexibility of the proposed system for multiple vehicle charging applications.

4.2. Dynamic and robustness evaluation

To evaluate the robustness of the proposed control system, disturbance tests were performed under the dual-output (SIDO) configuration to highlight the effectiveness of the four-loop master–slave strategy.

4.2.1. Load variation

In these tests, step-type disturbances of +20 V and −20 V were applied to the voltage of the first battery at 2 s and 4 s, respectively. As illustrated in Figure 10, the disturbance caused a temporary reduction in the current of the first battery and a corresponding deviation in its terminal voltage. Nevertheless, the voltage quickly recovered to its nominal value within approximately 100 ms, confirming the fast dynamic response of the proposed controller. The main reason for this fast recovery is the hierarchical cascaded control structure, which rapidly compensates for the disturbance in the inner current loop before the outer voltage loop brings the voltage back to the reference value of the battery. Importantly, both the current and voltage of the second battery remained unaffected, demonstrating the effective decoupling capability and disturbance rejection performance of the proposed control scheme under SIDO operation.

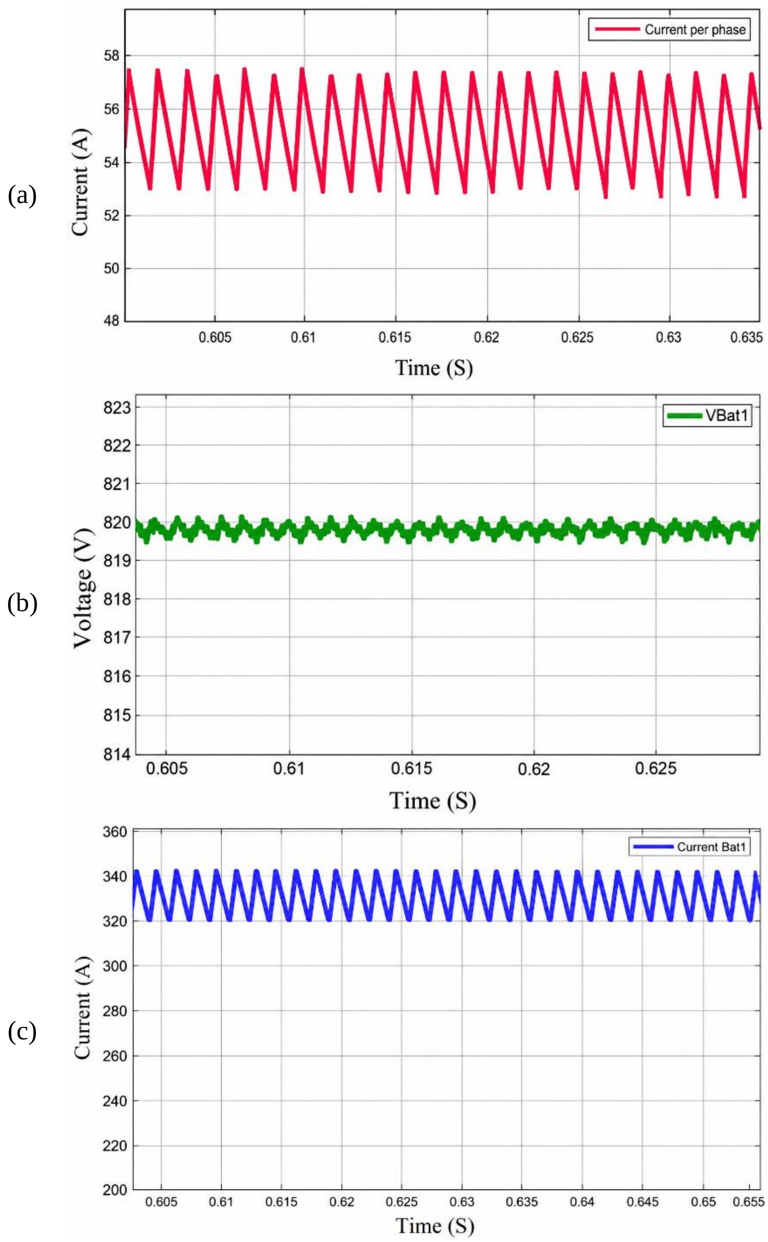

Figure 8. The steady-state waveforms of the proposed converter presented in Figure 2:
(a) inductor current of one phase, (b) output voltage, and (c) inductor currents of all interleaved phases

(a)

(b)

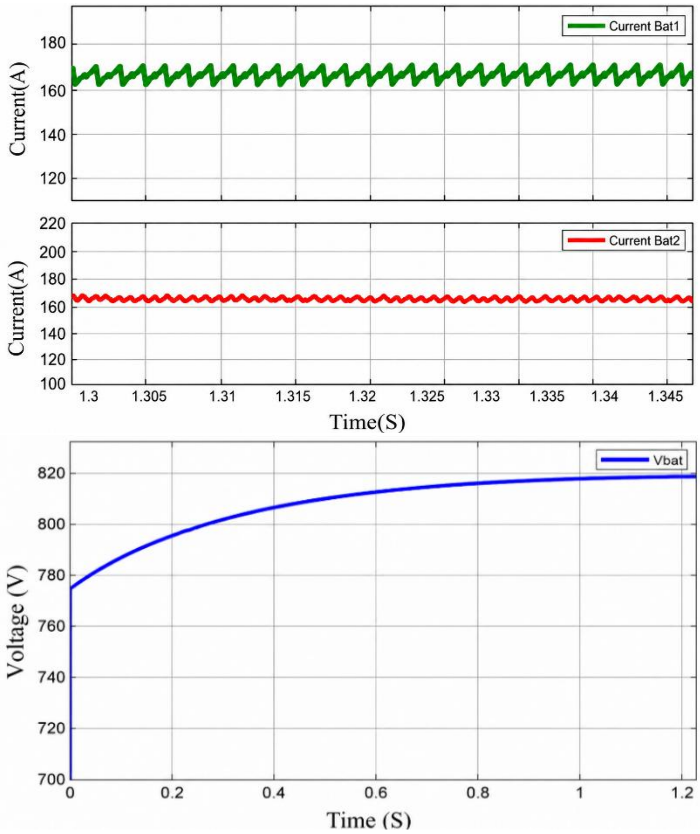

Figure 9. Steady-state waveforms of the proposed interleaved buck converter under dual-output operation: (a) inductor currents showing current sharing and (b) battery voltage

4.2.2. Input voltage variation

Figure 11 illustrates the system response under SIDO operation when subjected to input voltage disturbances. A step variation of 500 V was applied at t = 2 s (positive) and t = 4 s (negative). Both battery voltages and currents exhibit small transient deviations following the disturbances but recover to their nominal values within approximately 100 ms. The inductor currents of the six interleaved phases also show fast damping and balanced sharing. These results confirm the robustness of the proposed four-loop master–slave control scheme in maintaining stable dual-battery operation under severe input fluctuations. The cascaded control loops are responsible for a fast recovery of the charging variables. After the input voltage disturbance, the inner current loop rapidly corrects the transient current error, and the outer voltage loops slowly return the battery voltages towards their setpoint. During the transient period, the current sharing mechanism ensures equal currents in all six interleaved phases.

4.2.3. Uncertainties in parameters

The robustness of the proposed control strategy has also been verified by introducing parametric uncertainty in the inductances of the six interleaved phases. In this test, the inductance values were randomly varied within the interval of 3.3 mH to 5 mH, and the system response was evaluated through numerical simulations. As shown in Figure 12, the variations in inductance did not affect the terminal voltages or charging currents of either battery. Both outputs remained stable and well regulated, with the CC–CV charging protocol preserved despite the parameter deviations.

The behavior is largely explained by the independent operation of each channel and the democratic current-sharing algorithm used in the inner loop. As a result, the mismatch between the inductances only influences the dynamics of the local phase current and does not influence the output variables, which ensures accurate CC–CV charging and confirms the robustness of the proposed 4-loop control structure.

The controller of the proposed EV charging system has a number of practical benefits over the recently reported IBC-based EV charging systems [24], [25]. The first is that the cascaded control architecture is simplified as it now includes four coordinated control loops, rather than six, and therefore has less implementation complexity, without the loss of regulation accuracy. Secondly, the proposed strategy is different from past works, which were focused on single-output charging, because it enables both SISO and

SIDO operation in the same controller. Thirdly, the proposed master-slave configuration provides effective dynamic decoupling, such that disturbances or parameter variations in one charging output have little effect on the second output. These characteristics are obtained with output ripple less than 1%, balanced current sharing, overshoot less than 5%, and a settling time of around 100 ms.

(a)
(b)
(c)

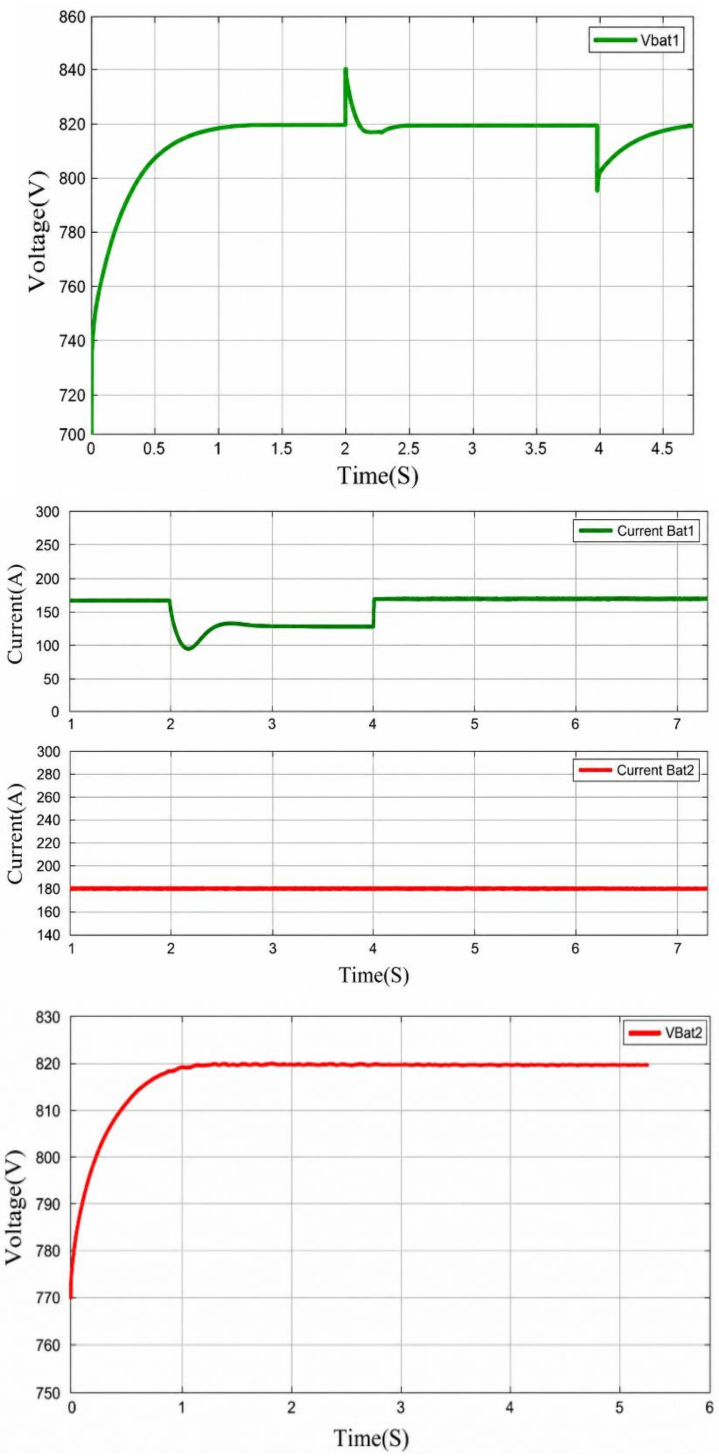

Figure 10. Dynamic response of the system under battery voltage disturbance:
(a) battery voltage $Vbat_1$, (b) inductor current IL, and (c) battery voltage Vbat

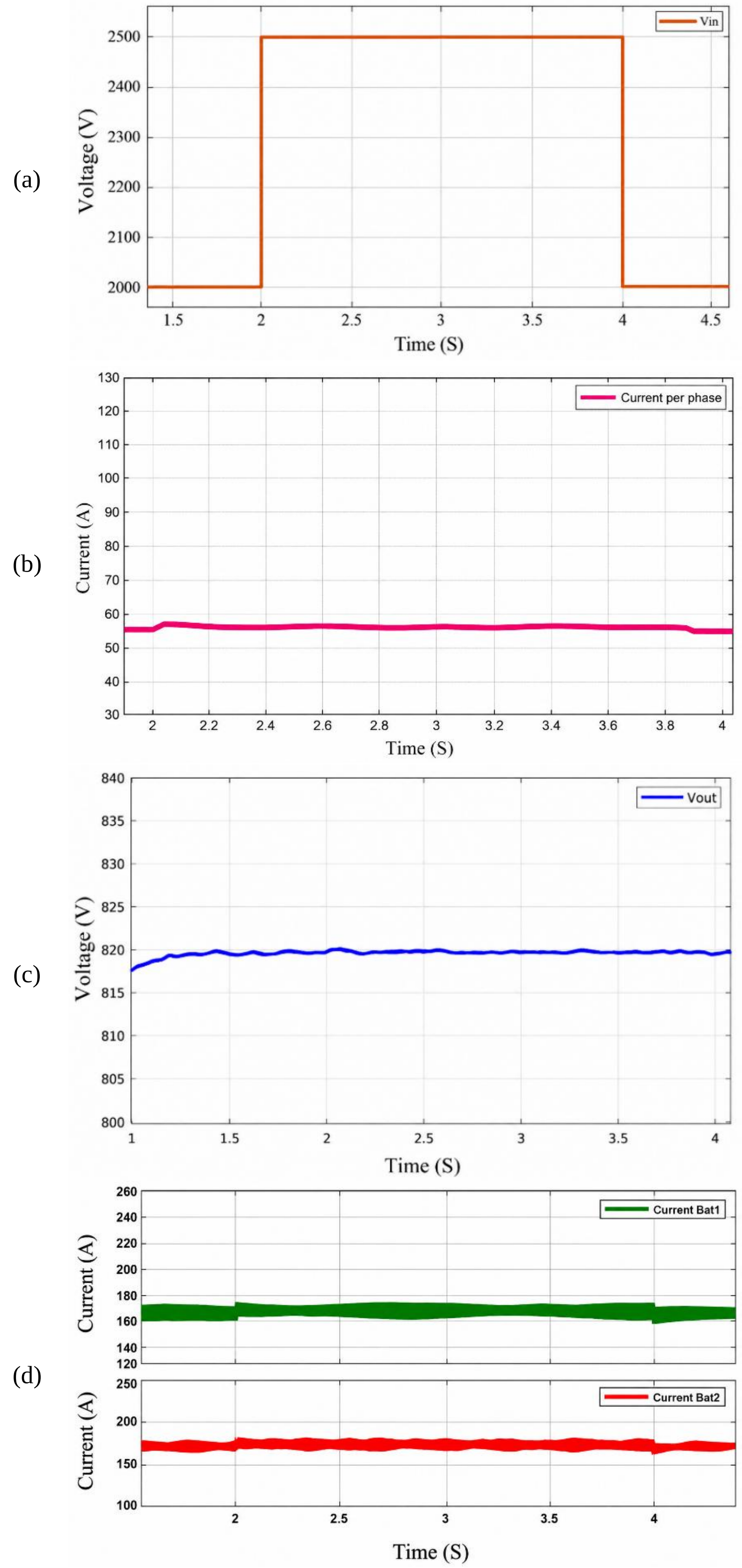

Figure 11. Dynamic response of the system under input voltage (Vin) step disturbance:
(a) input voltage, (b) inductor current IL, (c) battery voltage Vbat, and (d) battery current Ibat

(a)

(b)

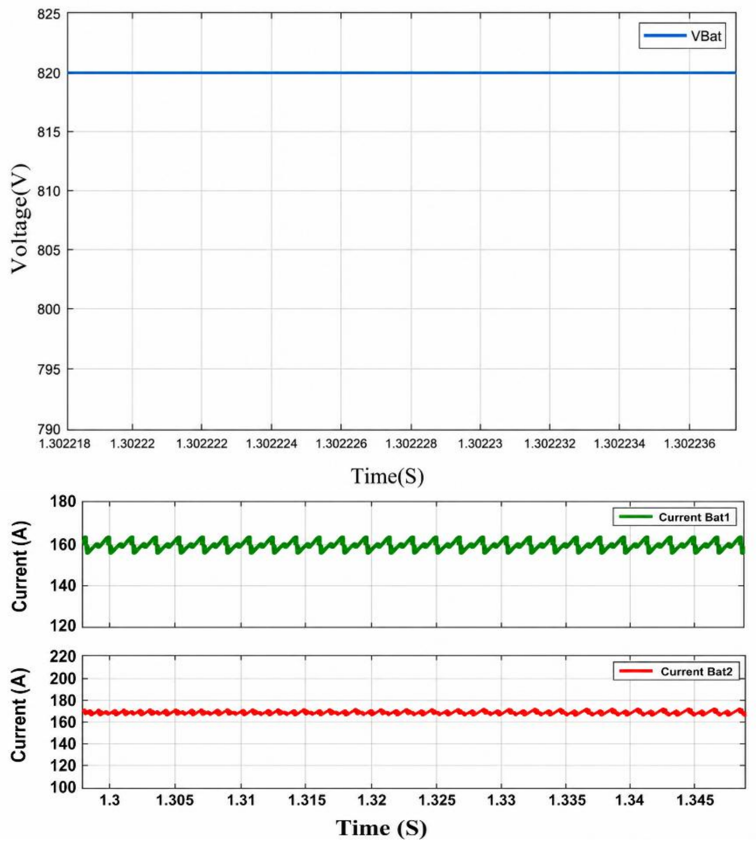

Figure 12. Effect of inductance mismatch among the interleaved phases on:
(a) battery voltage and (b) battery current

4.3. Grid interaction and standards compliance

The study does not explicitly consider grid-connected operation, but there is interaction with the utility grid that can be concluded from the behavior of the DC-bus and the output characteristics of the charging system. From a practical perspective, stable DC-bus regulation and smooth current profiles are key factors that affect the performance of the grid side. The results obtained show that the battery current and output voltage have low ripple levels and fast transient response when subjected to disturbances. These are qualities that help to minimize voltage fluctuations and harmonic distortion in the range of their grid connection via a front-end converter.

Hence, although not modeled directly in this work, the results obtained suggest the potential compatibility of the proposed control strategy with the requirements for integration with the grid. It is believed that the achieved low current ripple, stable DC-bus regulation, and fast transient response will help to meet the general requirements of IEC 61851 and IEEE 519. Detailed verification of harmonic performance and full compliance with the standards is considered as future work; however, it requires experimental validation on the grid.

5. CONCLUSION

A six-phase IBC is modeled and controlled for EV battery charging applications with ultrafast charging speed in this work. The multi-loop control strategy under the (CC–CV) charging scheme has been developed by cascading the PI controllers to achieve stable operation. One of the main features of this study is the reduction of the number of control loops from the conventional configuration of the control system to 4 coordinated loops to simplify the control architecture. This reduction makes calculations easier and enables implementation, while ensuring correct current sharing and stable voltage regulation. The simulation results show that the proposed system can maintain the battery voltage at around 820 V and the charging current at around 330 A, with low ripple. The dynamic performance indicates that the settling time is around 100ms with an overshoot less than 5%, and the frequency domain analysis is sufficient to ensure stability margins for both current and voltage control loops. Moreover, the proposed control approach has high robustness and fault tolerance. There are no significant changes in the other output due to disturbances, parameter changes, or faults to the first output - good decoupling between cascaded control loops. In multi-output (SIMO) EV charging systems, this behavior is used to guarantee operation. The results presented in the present work show that the proposed approach is suitable for high-performance EV charging applications, although validation is restricted to simulation. The proposed future work will involve experimental validation and the extension of the system to grid-connected operation, including detailed power quality analysis and compliance with practical standards.

FUNDING INFORMATION

No funding involved.

AUTHOR CONTRIBUTIONS STATEMENT

This journal uses the Contributor Roles Taxonomy (CRediT) to recognize individual author contributions, reduce authorship disputes, and facilitate collaboration.

Name of Author	C	M	So	Va	Fo	I	R	D	O	E	Vi	Su	P	Fu
Alya H. Al-Rifaie	✓	✓	✓		✓	✓		✓	✓		✓		✓	
Mohammed Obaid Mustafa		✓		✓	✓	✓	✓	✓		✓	✓	✓	✓	

C : **C**onceptualization
M : **M**ethodology
So : **So**ftware
Va : **Va**lidation
Fo : **Fo**rmal analysis
I : **I**nvestigation
R : **R**esources
D : **D**ata Curation
O : Writing - **O**riginal Draft
E : Writing - Review & **E**diting
Vi : **Vi**sualization
Su : **Su**pervision
P : **P**roject administration
Fu : **Fu**nding acquisition

CONFLICT OF INTEREST STATEMENT

We have no known conflicting financial interests or personal relationships that could influence the work reported in this paper.

DATA AVAILABILITY

We confirm that the data supporting the findings of this study are available within the article.

REFERENCES

[1] A. Cid-Pastor, L. Martinez-Salamero, C. Alonso, R. Leyva, and S. Singer, "Paralleling DC–DC switching converters by means of power gyrators," *IEEE Transactions on Power Electronics*, vol. 22, no. 6, pp. 2444–2453, Nov. 2007, doi: 10.1109/TPEL.2007.909311.

[2] O. Lopez-Santos, D. Zambrano-Prada, L. Martinez-Salamero, A. El Aroudi, and L. Vazquez-Seisdedos, "Unidirectional DC-DC converters for ultrafast charging of electric vehicles," in *2023 IEEE International Conference on Electrical Systems for Aircraft, Railway, Ship Propulsion and Road Vehicles & International Transportation Electrification Conference (ESARS-ITEC)*, IEEE, Mar. 2023, pp. 1–6. doi: 10.1109/ESARS-ITEC57127.2023.10114830.

[3] E. N. Mammeri, O. Lopez-Santos, A. El Aroudi, L. Martinez-Salamero, J. Domajnko, and N. Prosen, "Modeling and control of a 36-phase interleaved buck converter as an ultrafast battery charger," *IFAC-PapersOnLine*, vol. 58, no. 13, pp. 424–429, 2024, doi: 10.1016/j.ifacol.2024.07.519.

[4] N. Kumar and M. Kumar, "Modeling and characterization of n-phase interleaved buck converter with circuit parasitic for battery charging applications," *Electrical Engineering*, vol. 107, no. 4, pp. 5329–5339, Apr. 2025, doi: 10.1007/s00202-024-02347-2.

[5] S. K. Ram, S. Devassy, B. K. Verma, and S. Mishra, "Hardware implementation of interleaved DC-DC buck converter for li-ion battery charging," in *2023 9th IEEE India International Conference on Power Electronics (IICPE)*, IEEE, Nov. 2023, pp. 1–5. doi: 10.1109/IICPE60303.2023.10474734.

[6] A. Garg and M. Das, "High efficiency three phase interleaved buck converter for fast charging of EV," in *2021 1st International Conference on Power Electronics and Energy (ICPEE)*, IEEE, Jan. 2021, pp. 1–5. doi: 10.1109/ICPEE50452.2021.9358486.

[7] C. Gupta and M. Das, "Multiphase interleaved DC-DC converter for fast charging application of electric vehicles," in *2022 IEEE 16th International Conference on Compatibility, Power Electronics, and Power Engineering (CPE-POWERENG)*, IEEE, Jun. 2022, pp. 1–6. doi: 10.1109/CPE-POWERENG54966.2022.9880893.

[8] T. Ikeya *et al.*, "Multi-step constant-current charging method for an electric vehicle nickel/metal hydride battery with high-energy efficiency and long cycle life," *Journal of Power Sources*, vol. 105, no. 1, pp. 6–12, Mar. 2002, doi: 10.1016/S0378-7753(01)00907-7.

[9] L.-R. Chen, "A design of an optimal battery pulse charge system by frequency-varied technique," *IEEE Transactions on Industrial Electronics*, vol. 54, no. 1, pp. 398–405, Feb. 2007, doi: 10.1109/TIE.2006.888796.

[10] L.-R. Chen, S.-L. Wu, D.-T. Shieh, and T.-R. Chen, "Sinusoidal-ripple-current charging strategy and optimal charging frequency study for li-ion batteries," *IEEE Transactions on Industrial Electronics*, vol. 60, no. 1, pp. 88–97, Jan. 2013, doi: 10.1109/TIE.2012.2186106.

[11] L.-R. Dung, C.-E. Chen, and H.-F. Yuan, "A robust, intelligent CC-CV fast charger for aging lithium batteries," in *2016 IEEE 25th International Symposium on Industrial Electronics (ISIE)*, IEEE, Jun. 2016, pp. 268–273. doi: 10.1109/ISIE.2016.7744901.

[12] J. Jiang and C. Zhang, *Fundamentals and Applications of Lithium-ion Batteries in Electric Drive Vehicles*. 2015.

[13] M. Hammami, A. Viatkin, M. Ricco, and G. Grandi, "A DC/DC fast charger for electric vehicles with minimum input/output ripple based on multiphase interleaved converters," in *2019 International Conference on Clean Electrical Power (ICCEP)*, IEEE, Jul. 2019, pp. 187–192. doi: 10.1109/ICCEP.2019.8890200.

[14] S. Valedsaravi, A. El Aroudi, and L. Martínez-Salamero, "Review of solid-state transformer applications on electric vehicle DC ultra-fast charging station," *Energies*, vol. 15, no. 15, p. 5602, Aug. 2022, doi: 10.3390/en15155602.

[15] J. Domajnko, N. Prosen, E. N. Mammeri, O. Lopez-Santos, A. El Aroudi, and L. Martinez-Salamero, "Non-isolated interleaved buck converter for ultrafast charging of batteries," in *Seminario Anual de Automática, Electrónica Industrial e Instrumentación (SAAEI)*, 2023, pp. 1–6.

[16] H. Tu, H. Feng, S. Srdic, and S. Lukic, "Extreme fast charging of electric vehicles: a technology overview," *IEEE Transactions on Transportation Electrification*, vol. 5, no. 4, pp. 861–878, Dec. 2019, doi: 10.1109/TTE.2019.2958709.

[17] A. C. Schittler, D. Pappis, A. Campos, M. A. Dalla Costa, and J. Marcos Alonso, "Interleaved buck converter applied to high power HID lamps supplying: Design, modeling and control," in *2011 IEEE Industry Applications Society Annual Meeting*, IEEE, Oct. 2011, pp. 1–7. doi: 10.1109/IAS.2011.6074376.

[18] H. Mao, L. Yao, C. Wang, and I. Batarseh, "Analysis of inductor current sharing in nonisolated and isolated multiphase DC–DC converters," *IEEE Transactions on Industrial Electronics*, vol. 54, no. 6, pp. 3379–3388, Dec. 2007, doi: 10.1109/TIE.2007.905966.

[19] A. Colvero Schittler, D. Pappis, A. Campos, M. A. Dalla Costa, and J. M. Alonso, "Interleaved buck converter applied to high-power HID lamps supply: Design, Modeling and Control," *IEEE Transactions on Industry Applications*, vol. 49, no. 4, pp. 1844–1853, Jul. 2013, doi: 10.1109/TIA.2013.2258131.

[20] M. S. Hassan and A. A. Elbaset, "Small-signal MATLAB/Simulink model of DC-DC buck converter using state-space averaging method," in *17th International Middle-East Power System Conference (MEPCON'15), at: Mansoura University*, 2015, pp. 1–9. doi: 10.13140/RG.2.1.1129.7368.

[21] Y. Qiu, K. Yao, Y. Meng, M. Xu, F. C. Lee, and M. Ye, "Control-loop bandwidth limitations for multiphase interleaving buck converters," in *Nineteenth Annual IEEE Applied Power Electronics Conference and Exposition*, IEEE, 2004, pp. 1322–1328. doi: 10.1109/APEC.2004.1295994.

[22] R. W. Erickson and D. Maksimović, *Fundamentals of Power Electronics*. Switzerland: Springer, 2020.

[23] R. A. Aprilianto and R. M. Ariefianto, "Interleaving technique for improving conventional buck converter performance," in *2022 International Conference on Technology and Policy in Energy and Electric Power (ICT-PEP)*, IEEE, Oct. 2022, pp. 249–254. doi: 10.1109/ICT-PEP57242.2022.9988881.

[24] E. N. Mammeri, O. Lopez-Santos, A. El Aroudi, J. Domajnko, N. Prosen, and L. Martinez-Salamero, "Modeling and control of a three-phase interleaved buck converter as a battery charger," *IEEE Access*, vol. 13, pp. 18325–18345, 2025, doi: 10.1109/ACCESS.2025.3533032.

[25] A. S. Samosir, T. Sutikno, A. F. Huda, and L. Mardiyah, "Design and simulation of an electric vehicle charger with integrated interleaved boost converter and phase-shifted full-bridge converter using MATLAB/Simulink," *International Journal of Electrical and Computer Engineering (IJECE)*, vol. 16, no. 2, p. 687, Apr. 2026, doi: 10.11591/ijece.v16i2.pp687-698.

BIOGRAPHIES OF AUTHORS

Alya H. Al-Rifaie is an assistant professor in the Department of Electrical Engineering Techniques, Technical Engineering College, Mosul, Iraq. She received her B.Sc. and M.Sc. degrees from the University of Mosul, Iraq, in 2005 and 2008, respectively. She then joined the Technical College of Mosul, Northern Technical University, Mosul, Iraq. She has published numerous papers in international conferences and scientific journals, particularly in the field of renewable energy systems. Her research interests include renewable energy, hybrid power systems, HVDC, power system protection, and AC machines. She is currently pursuing her Ph.D. at the University of Mosul. She can be contacted at email: alya.23enp10@student.uomosul.edu.iq or alya.hamid@ntu.edu.iq.

Mohammed Obaid Mustafa is an assistant professor in the Department of Electrical Engineering at the University of Mosul, where he has been serving since 2022. He has also been a senior lecturer since 2015. He received his B.Eng. degree in electrical engineering and his M.Sc. degree in power and machines from the University of Mosul, Iraq, in 1998 and 2002, respectively. He obtained his Ph.D. degree in Automatic Control from Luleå University of Technology, Sweden, in 2015. His research interests include control systems, motor drives, industrial applications, and photovoltaic power systems. He can be contacted at email: mohammed.obaid@uomosul.edu.iq.